Proceedings of Global Power and Propulsion Society
ISSN-Nr: 2504-4400
GPPS Hong Kong 2023
October 17-19, 2023
www.gpps.global

GPPS-TC-2023-0093

Sound generation by entropy perturbations passing through circular orifices

Hanzhuo Zhang
Department of Mechanics and Aerospace Engineering, Southern University of Science and Technology
11912610@mail.sustech.edu.cn
Shenzhen, Guangdong, China

Dong Yang
Department of Mechanics and Aerospace Engineering, Southern University of Science and Technology
yangd3@sustech.edu.cn
Shenzhen, Guangdong, China

2023.7.24

ABSTRACT

Entropy waves generate sound in the presence of flow gradients. At the exit of a combustor, entropy noise generated by the acceleration of entropy waves may affect thermoacoustic stabilities inside the combustion chamber. The Cambridge EWG experiments measured the noise generated by entropy waves passing through a circular orifice. However, predictions based on isentropic models differed significantly from experiment results. To address this mismatch, a compact, one-dimensional model that considers the contraction effects at the throat and the degree of non-isentropic effect of the expansion section has been developed previously. However, this model does not explain the differences in acoustic response between thin and thick orifices. This work considers the influence of the L/D ratio of the holes on the internal flow state and corrects the vena contracta factor corresponding to the thick orifice in the previous model. The results of the modified model are closer to the experiment results than those of the previous model. Both theoretical and experimental results indicate that for orifices with small aperture ratios, the entropy noise reflection coefficient is less sensitive to the variation of the flow contracta factor compared to the acoustic reflection coefficient.

1. INTRODUCTION

Due to the strict requirement for low NOx emissions, lean premixed combustion is commonly used in both aviation and land-based gas turbines. However, this combustion method is more prone to thermoacoustic instabilities within the combustor, which seriously affects the reliability and safety of the gas turbines. Thermoacoustic instabilities come from the coupling with acoustic waves inside the combustion chamber and the unsteady heat release rate. Entropy waves generated by unsteady combustion can produce sound when flowing through structures with flow gradients, such as at the combustion chamber outlet and turbine blade rows. Part of the entropy noise will be reflected into the combustion chamber and couples

with the flame, which may lead to the occurrence of thermoacoustic instabilities (Morgans and Duran, 2016). Therefore, it is necessary to study the mechanism of entropy noise and quantitatively evaluate its impact on thermoacoustic instabilities.

Currently, there are two main approaches to modeling the entropy noise. The first approach starts by determining the acoustic sources related to entropy waves. Based on the acoustic analogy equation (Lighthill, 1952), this approach uses the control equations of the flow to determine the sound source term related to entropy perturbation. Representatives in this field include the work of Morfey and the work of Howe et al. (Morfey, 1973; Howe, 1975). The second approach starts by the assumptions of acoustic compactness, quasi-one-dimensional flow, small perturbations, and isentropic processes. Based on perturbation theory, this approach solves the transfer function related to entropy perturbations. Mabel and Candel's work is representative of this approach (Marble and Candel, 1977).

Experimental measurements are a powerful tool for verifying the accuracy of the aforementioned models. DLR has built an experimental setup with an entropy wave generator (Bake et al., 2009), which avoids the complex conditions of a real combustion chamber. The entropy wave generator produces entropy waves by perturbing the heat release rate through an electric heating device, and the entropy waves are accelerated through a convergent-divergent nozzle. Due to the difference between the convection velocity and the speed of sound, the time for the acoustic signals caused by entropy noise and direct noise to reach the measurement point is different, and this can be used to distinguish between the two types of noise. However, there is controversy in the academic community regarding the analysis of the results of this experiment (Morgans and Duran, 2016), and additional experiments are conducted by Domenico et al. and Rolland et al. at the University of Cambridge (De Domenico et al., 2017a; Rolland et al., 2017; De Domenico et al., 2017b). The main difference between their experiments and DLR's EWG experiment is that they used an orifice instead of a convergent-divergent nozzle, and the measurement location was moved upstream of the acceleration region to measure the direct noise and the reflected entropy noise. The experiment results indicate that in the case of subsonic Mach numbers in the throat of orifices, the contribution of entropy-induced noise may not be negligible compared to that of the direct noise, but the value of the indirect noise obtained from the experiment is significantly higher than the results of existing isentropic models.

Domenico et al. have then developed a non-isentropic compact quasi-one-dimensional theoretical model to predict entropy noise (De Domenico et al., 2019), which is in good agreement with experiment results. The model considers the contraction effect of the flow inside the orifice by introducing the vena contracta factor Γ and a model parameter β to measure the non-isentropic degree of flow expansion. This model has been shown to be able to predict the response of orifices and nozzles to acoustic perturbations. The vena contracta factor of the orifice is determined by Durrieu's model (Durrieu et al., 2001), which is a function of the throat Mach number and increases with the throat Mach number. However, this model assumes that the vena contracta factors of the nozzle at different throat Mach numbers are equal to the vena contracta factor corresponding to the choked state of the nozzle ($\Gamma = 0.9$) without considering the impact of the throat Mach number. Therefore, the determination of the vena contracta factor of the nozzle in this model may be not accurate enough. Moreover, due to the sudden change in the cross-sectional area of the orifice, the degree of flow contraction should be more severe, and the vena contracta factor should be smaller than that of the nozzle with a gradually varying cross-sectional area. Cambridge's experiment results also show that the vena contracta factor of the thin orifice is significantly lower than that of the nozzles with the same hole diameter, but the vena contracta factor of the thick orifice with the same hole diameter is different from that of the thin orifice and is compared to that of the nozzle. Besides, the acoustic reflection coefficient of a thick orifice is similar to that of a nozzle, while the difference between the acoustic reflection coefficients of thick and thin orifices is significant under identical inflow conditions. However, the non-isentropic model from Domenico et al. cannot explain this phenomenon. Therefore, the present study makes a modification based on the Cambridge model specifically for the thick orifice and uses this to explain the above phenomenon.

This article has three main contributions. Firstly, a modified entropy noise model for orifices are developed based on the Cambridge model for thick orifices. The predicted acoustic reflection coefficient values obtained from this model are found to be closer to experiment results, indicating the need to consider flow reattachment effects. Secondly, through the study of the sensitivity of two reflection coefficients to the equivalent contraction ratio, it is found that the acoustic

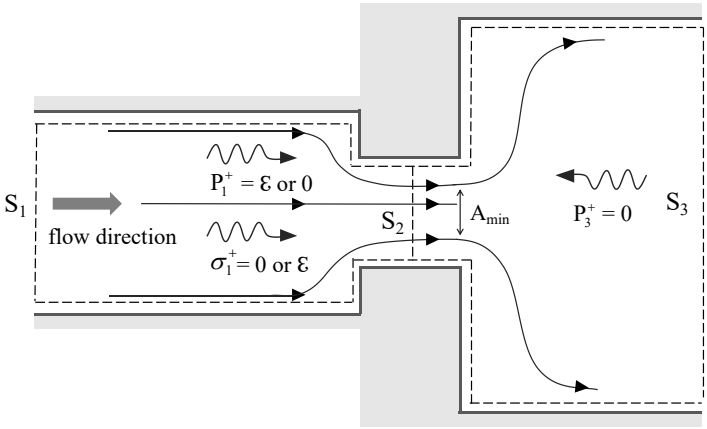

Figure 1 Flow passing through the orifice plate

reflection coefficient is more sensitive to the vena contracta factor than the entropy noise reflection coefficient. Further analysis shows that the trends of both reflection coefficients with the equivalent contraction ratio are consistent and exhibit a nonlinear relation between reflection coefficients and the throat Mach number.

The organization of this paper is as follows: in Section 2, an entropy noise model applicable to thick orifices (with large hole length-to-diameter ratios) is developed by modifying the Cambridge model. In Section 3, the results of three theoretical models are compared with experiment results, demonstrating the importance to consider flow reattachment effects caused by large orifice thickness. The sensitivity of both acoustic and entropy noise reflection coefficients to the equivalent contraction ratio and relevant analysis are discussed. Conclusions are given in section 4.

2. MODELING

The flow passing through the orifice plate is illustrated in Figure 1. Flow contraction may occur at the inlet of the orifice (Durrieu et al., 2001), which can be considered by introducing the parameter Γ, where $\Gamma = A_{min}/A_2$ and A_{min} represents the minimum cross-sectional area of the flow inside the throat. However, according to previous studies, for orifices with a relatively large length-to-diameter ratio, flow reattachment will occur inside the orifice (Brokof et al., 2023).

In the Cambridge experiment, the hole length for the thick plate is 8mm, while for the thin plate, it is only 2.2mm. Both orifices have the same diameter of 6.6mm and the L/D value of the thick orifice is around 1.2 which is nearly 4 times that of the thin orifice. Therefore, we assume that flow reattachment occurs inside the orifice of the thick orifice, and the vena contracta factor Γ can be approximated as 1, rather than the 0.9 assumed in the previous non-isentropic model. In contrast, for the thin orifice, there is no flow reattachment, and the vena contracta factor should be less than 1. In order to verify the above hypotheses, it is necessary to model and conduct further analysis. The modeling process refers to previous studies：(De Domenico et al., 2019; Guzmán-Iñigo et al., 2022)

The control volume is selected as the region enclosed by the dashed line in the Figure 1, where the cross-sections S_1 and S_3 are far away from the orifice to ensure that the flow where can be approximated as one-dimensional. The flow state at the throat cross-section S_2 is also assumed to be one-dimensional, and A_1, A_2, and A_3 correspond to the cross-sectional areas at the three sections. Moreover, it is assumed that the perturbation frequency is sufficiently low, so the flow inside the control volume can be considered quasi-steady. Additionally, the boundary conditions at the wall are assumed to be adiabatic and frictionless. Thus, the flow passing through the orifice satisfies the conservation of mass and energy.

For thick orifice ($\Gamma = 1$), mass and energy conservation among S_1, S_2 and S_3 gives:

$$\rho_1 u_1 A_1 = \rho_2 u_2 A_2, \qquad h_{t,1} = h_{t,2}, \tag{1a}$$

$$\rho_2 u_2 A_2 = \rho_3 u_3 A_3, \qquad h_{t,2} = h_{t,3}, \tag{1b}$$

Where ρ_i represents density, u_i represents flow velocity, and $h_{t,i}$ means stagnation enthalpy.

Due to the fact that the pressure gradient of the contracting flow is favorable, the boundary layer is less likely to separate. Therefore, the flow between S_1 and S_2 can be considered to be isentropic (De Domenico et al., 2019), that is:

$$\frac{P_1}{\rho_1^\gamma} = \frac{P_2}{\rho_2^\gamma} \tag{2}$$

Where P_i represents pressure and γ is the heat capacity ratio.

For the flow expansion, as the pressure gradient is adverse, the boundary layer separates, and the isentropic condition is no longer satisfied. The momentum conservation equation for the flow between S_2 and S_3 is used (Guzmán-Iñigo et al., 2022):

$$\rho_2 u_2^2 A_2 + p_2 A_3 = \left(\rho_3 u_3^2 + p_3\right) A_3 \tag{3}$$

If consider a thin orifice, the contraction effect of the flow at the throat needs to be taken into account, then part of equations (1a), (1b), and (3) can be modified by:

$$\rho_1 u_1 A_1 = \rho_2 u_2 A_2 \Gamma, \;\; \rho_2 u_2 A_2 \Gamma = \rho_3 u_3 A_3, \tag{4}$$

$$\rho_2 u_2^2 A_2 \Gamma + p_2 A_3 = \left(\rho_3 u_3^2 + p_3\right) A_3, \tag{5}$$

Given the mean flow conditions at S_1, mean flow parameters at S_2 and S_3 can be resolved through Eqs. (1-5). By writting flow parameters as the sum of a mean part denoted by $\bar{(\cdot)}$, and a much smaller perturbation denoted by $\hat{(\cdot)}$, Subtracting the mean part from the overall equation and keeping only the first-order perturbation terms, the linearized form of Eqs. (1-5) can be written as:

Between cross-section S_1 and S_2:

$$\left[(1+M_1)P_1^+ + (M_1-1)P_1^- - M_1\sigma_1\right]\eta_{1,2} = \lambda_{1,2}\phi_{1,2}\left[(1+M_2)P_2^+ + (M_2-1)P_2^- - M_2\sigma_2\right] \tag{6a}$$

$$\sigma_1 = \sigma_2 \tag{6b}$$

$$(\gamma-1)(1+M_1)P_1^+ + (\gamma-1)(1-M_1)P_1^- + \sigma_1 = \phi_{1,2}^2\left[(\gamma-1)(1+M_2)P_2^+ + (\gamma-1)(1-M_2)P_2^- + \sigma_2\right] \tag{6c}$$

Between cross-section S_2 and S_3:

$$\left[(1+M_2)P_2^+ + (M_2-1)P_2^- - M_2\sigma_2\right]\eta_{2,3} = \lambda_{2,3}\phi_{2,3}\left[(1+M_3)P_3^+ + (M_3-1)P_3^- - M_3\sigma_3\right] \tag{7a}$$

$$\begin{aligned}\left(\eta_{2,3}\left((1+M_2)^2-1\right)+1\right)P_2^+ - \left(\eta_{2,3}\left(1-(1+M_2)^2\right)-1\right)P_2^- - \eta_{2,3}M_2^2\sigma_2 \\ = \lambda_{2,3}\phi_{2,3}^2\left((1+M_3)^2P_3^+ + (1-M_3)^2P_3^- - M_3^2\sigma_3\right)\end{aligned} \tag{7b}$$

$$(\gamma-1)(1+M_2)P_2^+ + (\gamma-1)(1-M_2)P_2^- + \sigma_2 = \phi_{2,3}^2\left[(\gamma-1)(1+M_3)P_3^+ + (\gamma-1)(1-M_3)P_3^- + \sigma_3\right] \tag{7c}$$

Where $P^+ = \left(\frac{\hat{p}}{\gamma\bar{p}} + \frac{\hat{u}}{c}\right)/2$ and $P^- = \left(\frac{\hat{p}}{\gamma\bar{p}} - \frac{\hat{u}}{c}\right)/2$ are acoustic waves propagating downstream and upstream, $\sigma = \frac{\hat{s}}{c_p}$ is the entropy wave advected downstream. Moreover, M_i represents the Mach number and c_i represents local sound speed, the cross-sectional area ratio between sections i and j is represented by $\eta_{i,j} = \frac{A_i}{A_j}$, the density ratio is $\lambda_{i,j} = \frac{\rho_j}{\rho_i}$ and $\phi_{i,j} = \frac{c_j}{c_i}$ represents sound speed ratio.

Equations (6) and (7) are derived under the assumption of $\Gamma = 1$. For the case where $\Gamma < 1$, as shown in Figure 1, the contraction $\eta_{1,2}$ and $\eta_{2,3}$ in Equations (6) and (7) corresponding to sections 1-2 and 2-3 can be replaced by equivalent contraction ratios $\eta'_{1,2} = \frac{\eta_{1,2}}{\Gamma}$ and $\eta'_{2,3} = \eta_{2,3}\Gamma$, respectively. In addition, since $\eta_{2,3} \to 0$ for orifices, the vena contracta factor Γ has a negligible effect on the flow in the expansion section.

The Cambridge EWG experimental setup can generate two independent sets of perturbations inlet conditions upstream of the orifices, as shown in Figure 1: the first set consists of only the upstream incident acoustic perturbation P_1^+ propagating

downstream, with no acoustic perturbation P_3^- propagating upstream and entropy perturbation σ_1. When the acoustic perturbation P_1^+ passes through the orifice, it generates reflection and transmission, and this case is used to study the acoustic response of the orifice to acoustic perturbations. The acoustic reflection coefficient R_1 can be defined as $R_1 = P_1^- / P_1^+$. The second set consists of only the incident entropy perturbation σ_1, with no upstream and downstream incident acoustic perturbation. When the incident entropy perturbation σ_1 passes through the orifice, it also generates reflection and transmission, and this case is used to study the acoustic response of the orifice to entropy perturbations. The entropy noise reflection coefficient R_s can be defined as $R_s = P_1^- / \sigma_1$.

Combining equations (6) and (7) with the three given incident waves P_1^+, σ_1, P_3^-, the remaining waves can be obtained by:

$$Y = \mathbf{T}^{-1} X \tag{8}$$

with

$$\mathbf{T} = \begin{bmatrix} \eta_{1,2}(1-M_1) & \lambda_{1,2}\phi_{1,2}(1+M_2) & -\lambda_{1,2}\phi_{1,2}(1-M_2) & -\lambda_{1,2}\phi_{1,2}M_2 & 0 & 0 \\ 0 & 0 & 0 & 1 & 0 & 0 \\ -(\gamma-1)(1-M_1) & \phi_{1,2}^2(\gamma-1)(1+M_2) & \phi_{1,2}^2(\gamma-1)(1-M_2) & \phi_{1,2}^2 & 0 & 0 \\ 0 & \eta_{2,3}(1+M_2) & \eta_{2,3}(M_2-1) & -\eta_{2,3}M_2 & -\lambda_{2,3}\phi_{2,3}(1+M_3) & \lambda_{2,3}\phi_{2,3}M_3 \\ 0 & \eta_{2,3}\left((1+M_2)^2-1\right)+1 & -\left(\eta_{2,3}\left(1-(1+M_2)^2\right)-1\right) & -\eta_{2,3}M_2^2 & -\lambda_{2,3}\phi_{2,3}^2(1+M_3)^2 & \lambda_{2,3}\phi_{2,3}^2M_3^2 \\ 0 & (\gamma-1)(1+M_2) & (\gamma-1)(1-M_2) & 1 & -\phi_{2,3}^2(\gamma-1)(1+M_3) & -\phi_{2,3}^2(\gamma-1)(1-M_3) \end{bmatrix} \tag{9}$$

and

$$X = \begin{bmatrix} \eta_{1,2}(1+M_1)P_1^+ - \eta_{1,2}M_1\sigma_1 \\ \sigma_1 \\ (\gamma-1)(1+M_1)P_1^+ + \sigma_1 \\ \lambda_{2,3}\phi_{2,3}(M_3-1) \\ \lambda_{2,3}\phi_{2,3}^2(1-M_3)^2 p_3^- \\ \phi_{2,3}^2\sigma_1 \end{bmatrix} \tag{10}$$

Where $Y = \begin{bmatrix} P_1^- & P_2^+ & P_2^- & \sigma_2 & P_3^+ & \sigma_3 \end{bmatrix}^T$.

3. Results and Discussion

Compare the results from the present model, the previous non-isentropic model and an isentropic model that only considers the contraction section (Rolland et al., 2017) with experiment results. The comparison is shown in Figure 2. For the acoustic reflection coefficient R_1 of the thick orifice, the present model's results are slightly higher than the experiment values, but closer to the experiment results than the results from the Cambridge model. For the entropy noise reflection coefficient R_s of the thick orifice, the results of the present model are in good agreement with the experiment values. Therefore, it can be inferred that the vena contracta factor for the thick orifice is closer to 1 rather than the 0.9 used by the Cambridge model. In addition, Figure 2(a) indicates that the vena contracta factors for the thin orifice at different incoming Mach numbers may be between 0.6 and 0.8.

Furthermore, the experiment results from Cambridge suggest that R_s may be less sensitive to the vena contracta factor than R_1 (as shown in Figure 1). As the vena contracta factor and the equivalent contraction ratio have a one-to-one correspondence, the sensitivity of the two reflection coefficients to the vena contracta factor Γ can be transformed into the influence of the variation of the equivalent contraction ratio ($\eta'_{1,2}$) on the two reflection coefficients. The results are shown in Figure 3. The sensitivities of R_1 and R_s to the equivalent contraction ratio are defined as α_R, and α_S, respectively. These values represent the absolute value of the gradient of the reflection coefficient divided by the reflection coefficient itself (taking the acoustic reflection coefficient as an example): $\alpha_R = \lim_{\delta\eta'_{1,2}\to 0} \left| \frac{\delta R_1}{R_1} \right| / \delta\eta'_{1,2} = |k_R / R_1|$. Where k_R represents the

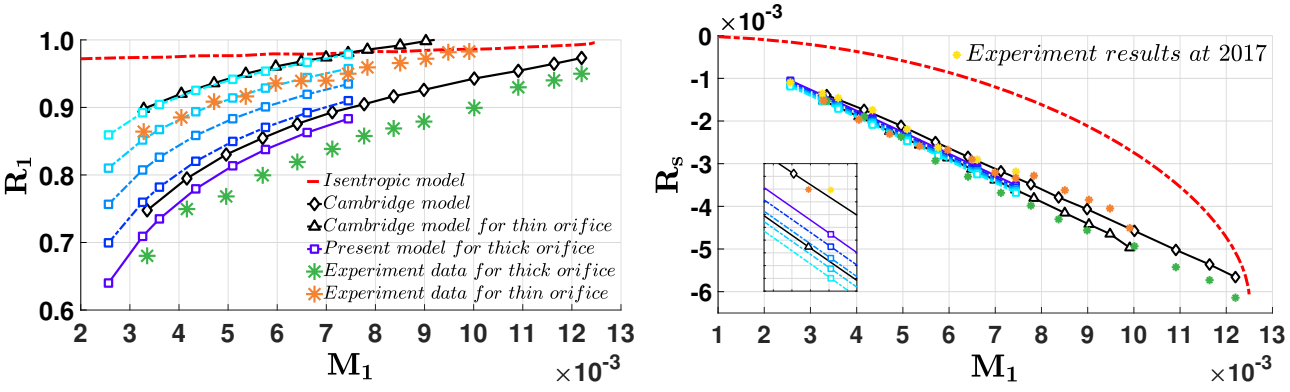

(a) **acoustic reflection coefficient** R_1 (b) **entropy noise reflection coefficient** R_s

Figure 2 The variation of reflection coefficients with upstream Mach number M_1, The vena contracta factor Γ for the thick orifice in both the isentropic and Cambridge models is 0.9. In the Cambridge model, the vena contracta factor for the thin orifice varies with the incoming Mach number M1. In the present model, the vena contracta factor for the thick orifice is 1. To estimate the vena contracta factor for the thin orifice using the present model, additional values of $\Gamma = 0.6, 0.7, 0.8, 0.9$ are considered. These values correspond to different blue and green dashed lines in the (a) from top to bottom, respectively.

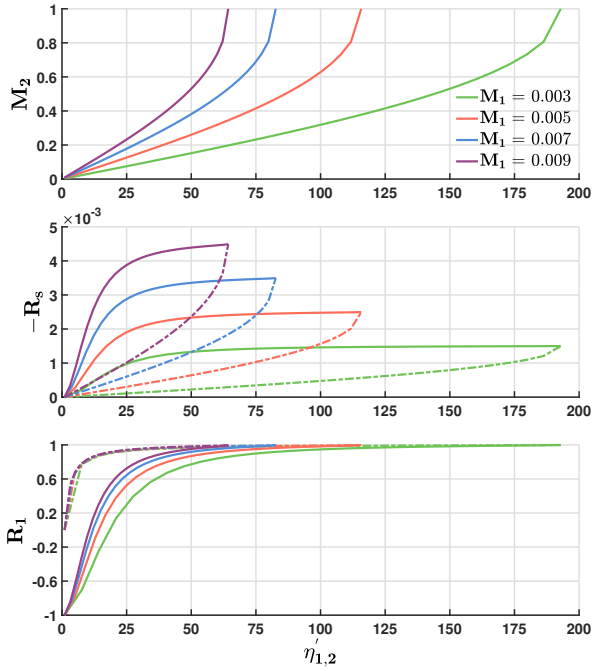

Figure 3 Reflection coefficients and throat Mach number variation with the change of equivalent contraction ratio.Dashed lines: isentropic subsonic predictions ;solid lines: results obtained from the current model.

slope of the curve showing the variation of the acoustic reflection coefficient R_1 with the change in the equivalent contraction ratio. Normalizing R_1 and R_s using $|R_{1,max}|$ and $|R_{s,min}|$, respectively, resulting in the normalized values $\tilde{R_1}$ and $\tilde{R_s}$ (as shown in Figure 4(a)), As a result, $\alpha_R/\alpha_S = (\tilde{k_R}/\tilde{R_1})/(\tilde{k_S}/\tilde{R_s})$. Subsequently, the normalised R_1 curve is shifted upwards, setting the minimum value to zero, with an upward shift of $x = |R_{1,min}/R_{1,max}|$, where $R_{1,min} = -1, R_{1,max} < 1$, thus, $x > 1$. Upon additional normalisation of the $\tilde{R_1}$ curve, resulting in the normalized values $\hat{R_1}$, it is found that the transformed curves for R_1 and R_s are identical. (as shown in Figure 4(b)). Therefore, for the same values of M_1 and $\eta^{'}$, $\tilde{k_R}$ and $\tilde{k_S}$ satisfy $\tilde{k_R} = (x+1)\tilde{k_S}$; $\tilde{R_1}$ and $\tilde{R_S}$ satisfy $\tilde{R_1} + x = (x+1)\tilde{R_S}$. Consequently, $\alpha_R/\alpha_S = \left|1 + x/\tilde{R_1}\right|, (-x < \tilde{R_1} < 1)$. When $\tilde{R_1} > 0$, $\alpha_R/\alpha_S > 2$; when $-\frac{x}{2} < \tilde{R_1} < 0$, $\alpha_R/\alpha_S > 1$; for $-1 < \tilde{R_1} < -\frac{x}{2}$, $0 < \alpha_R/\alpha_S < 1$. The findings suggest that when the acoustic reflection coefficient is positive (e.g., for orifices with small aperture ratios), the entropy noise reflection coefficient R_s is relatively

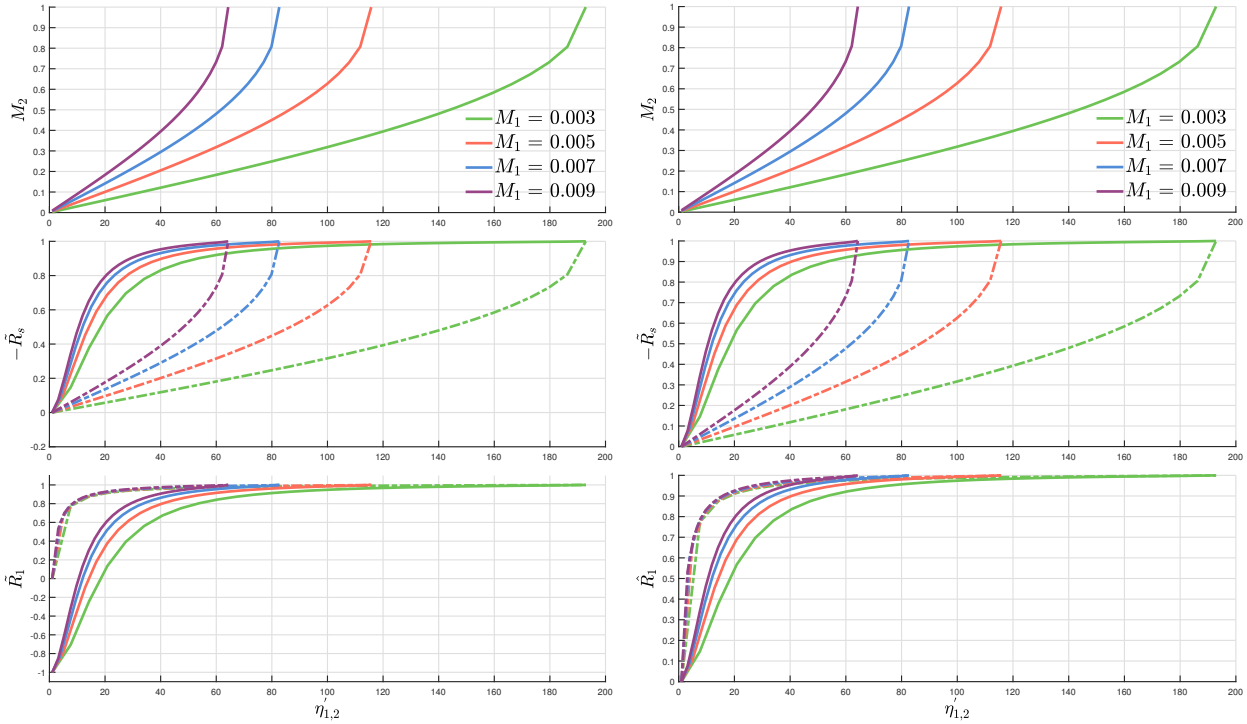

(a) (b)

Figure 4 Normalization is applied to both reflection coefficients.

less sensitive compared to the acoustic reflection coefficient R_1 with respect to the variation of the flow contracta factor. Moreover, this conclusion holds true for subsonic flow conditions (not include). However, the specific reasons behind this require further research.

In addition, the reason why the entropy noise reflection coefficient obtained from the isentropic model is lower than the results of the present model may be due to the fact that the downstream flow expansion is not considered in the isentropic model. At the orifice exit, the sound wave will be reflected due to the sudden expansion, and a portion of the sound energy will be reflected back upstream.

Moreover, from Figure 3 and data under other incoming Mach numbers M_1 (not included), the trends of the change in the acoustic reflection coefficient and the entropy noise reflection coefficient with respect to the equivalent contraction ratio are similar. For the same incoming Mach number M_1, both reflection coefficients have a nonlinear relationship with the throat Mach number M_2. For example, in Figure 3, when the incoming Mach number $M_1 = 0.003$ and the throat Mach number approaches 0.2, the entropy noise reflection coefficient R_s has already approximately converged to its maximum value $R_{s,max}$.

4. CONCLUSION

In this paper, we developed a theoretical model to predict the noise generated by entropy perturbations passing through a circular thick orifice by modifying the Cambridge model and correcting the vena contracta factor of the thick orifice to 1. The predicted acoustic reflection coefficients obtained from the present model are closer to the experiment results, indicating that the influence of different flow states inside the orifice hole caused by different hole lengths on the acoustic response characteristics of the orifice is worth considering. By studying the sensitivities of the acoustic reflection coefficient and the entropy noise reflection coefficient to the equivalent contraction ratio, it is demonstrated that when the acoustic reflection coefficient of the orifice is positive (such as in the case of orifices with small aperture ratios), the entropy noise reflection coefficient R_s is less sensitive to the variation of the flow contracta factor compared to the acoustic reflection coefficient R_1. Besides, it is found that the trends of the two reflection coefficients with the equivalent contraction ratio are similar,

and both reflection coefficients have a nonlinear dependence on the throat Mach number M_2. The specific reasons for this require further exploration.

NOMENCLATURE

α	the sensitivity of the reflection coefficient to the equivalent contraction ratio
β	a parameter is introduced to quantify the pressure losses and entropy gains
η	contraction ratio
Γ	vena contracta factor
γ	heat capacity ratio
λ	density ratio
$\mathbf{T}$	wave transfer matrix
ϕ	sound speed ratio
ρ	density
σ	dimensionless entropy perturbation
A	cross-section area
b	a specific value of equivalent contraction ratio
c	a specific value of dimensionless reflection coefficient
c	sound speed
c_p	heat capacity at constant pressure, J / (K · kg)
d	a specific value of dimensionless reflection coefficient
h	enthalpy
k	the slope of the curve showing the variation of the reflection coefficient with the change of the equivalent contraction ratio
M	Mach number
P	dimensionless pressure
p	pressure
R	reflection coefficient
S	cross-section
s	entropy
T	temperature
u	velocity
X	input condition vector
Y	output wave vector
Superscripts	
$'$	equivalent
$+$	downstream propagation
$-$	upstream propagation
Overscripts	
$\bar{}$	mean value
$\hat{}$	perturbation value
$\tilde{}$	normalized value by its maximum
Subscripts	
$1,2,3$	section number
max	maximum quantity
min	minimum quantity
t	stagnation

ACKNOWLEDGMENTS

The author would like to thank the National Natural Science Foundation of China (NO.52106159) for supporting this research.

References

Bake, F., Richter, C., Mühlbauer, B., Kings, N., Röhle, I., Thiele, F. and Noll, B. (2009), 'The entropy wave generator (ewg): a reference case on entropy noise', Journal of Sound and Vibration **326**(3-5), 574–598.

Brokof, P., Guzmán-Iñigo, J., Yang, D. and Morgans, A. S. (2023), 'The acoustics of short circular holes with reattached bias flow', Journal of Sound and Vibration **546**, 117435.

De Domenico, F., Rolland, E. O. and Hochgreb, S. (2017a), 'Detection of direct and indirect noise generated by synthetic hot spots in a duct', Journal of Sound and Vibration **394**, 220–236.

De Domenico, F., Rolland, E. O. and Hochgreb, S. (2017b), Measurements of the effect of boundary conditions on upstream

and downstream noise arising from entropy spots, in 'Turbo Expo: Power for Land, Sea, and Air', Vol. 50800, American Society of Mechanical Engineers, p. V02CT43A009.

De Domenico, F., Rolland, E. O. and Hochgreb, S. (2019), 'A generalised model for acoustic and entropic transfer function of nozzles with losses', Journal of Sound and Vibration **440**, 212–230.

Durrieu, P., Hofmans, G., Ajello, G., Boot, R., Aurégan, Y., Hirschberg, A. and Peters, M. (2001), 'Quasisteady aero-acoustic response of orifices', The Journal of the Acoustical Society of America **110**(4), 1859–1872.

Guzmán-Iñigo, J., Yang, D., Gaudron, R. and Morgans, A. S. (2022), 'On the scattering of entropy waves at sudden area expansions', Journal of Sound and Vibration **540**, 117261.

Howe, M. (1975), 'Contributions to the theory of aerodynamic sound, with application to excess jet noise and the theory of the flute', Journal of fluid mechanics **71**(4), 625–673.

Lighthill, M. J. (1952), 'On sound generated aerodynamically i. general theory', Proceedings of the Royal Society of London. Series A. Mathematical and Physical Sciences **211**(1107), 564–587.

Marble, F. and Candel, S. (1977), 'Acoustic disturbance from gas non-uniformities convected through a nozzle', Journal of sound and vibration **55**(2), 225–243.

Morfey, C. (1973), 'Amplification of aerodynamic noise by convected flow inhomogeneities', Journal of Sound and Vibration **31**(4), 391–397.

Morgans, A. S. and Duran, I. (2016), 'Entropy noise: A review of theory, progress and challenges', International Journal of Spray and Combustion Dynamics **8**(4), 285–298.

Rolland, E., De Domenico, F. and Hochgreb, S. (2017), 'Theory and application of reverberated direct and indirect noise', Journal of Fluid Mechanics **819**, 435–464.